Journal of Power Sources 196 (2011) 1469–1473

Contents lists available at ScienceDirect

Journal of Power Sources

journal homepage: www.elsevier.com/locate/jpowsour

Short communication

SnCo nanowire array as negative electrode for lithium-ion batteries

Germano Ferrara [a], Libero Damen [b], Catia Arbizzani [b], Rosalinda Inguanta [a], Salvatore Piazza [a], Carmelo Sunseri [a], Marina Mastragostino [b,*]

[a] Università degli Studi di Palermo, Dipartimento di Ingegneria Chimica dei Processi e dei Materiali, Viale delle Scienze Ed. 6, 90128 Palermo, Italy
[b] Università degli Studi di Bologna, Dipartimento di Scienza dei Metalli, Elettrochimica e Tecniche Chimiche, Via San Donato 15, 40127 Bologna, Italy

ARTICLE INFO

Article history:
Received 26 July 2010
Received in revised form 3 September 2010
Accepted 16 September 2010
Available online 22 September 2010

Keywords:
Tin
Tin–cobalt alloy
Nanowire
Anode
Lithium-ion battery

ABSTRACT

Amorphous SnCo alloy nanowires (NWs) grown inside the channels of polycarbonate membranes by potentiostatic codeposition of the two metals (SnCo-*PM*) were tested vs. Li by repeated galvanostatic cycles in ethylene carbonate-dimethylcarbonate – $LiPF_6$ for use as negative electrode in lithium ion batteries. These SnCo electrodes delivered an almost constant capacity value, near to the theoretical for an atomic ratio Li/Sn of 4.4 over more than 35 lithiation–delithiation cycles at 1 C. SEM images of fresh and cycled electrodes showed that nanowires remain partially intact after repeated lithiation–delithiation cycles; indeed, several wires expanded and became porous. Results of amorphous SnCo nanowires grown inside anodic alumina membranes (SnCo-*AM*) are also reported. The comparison of the two types of NW electrodes demonstrates that the morphology of the SnCo-*PM* is more suitable than that of the SnCo-*AM* for electrode stability over cycling. Optimization of NW technology should thus be a promising route to enhancing the mechanical strength and durability of tin-based electrodes.

1. Introduction

The demand to enhance the performance and safety of lithium-ion batteries has stimulated the search for anode materials as alternatives to graphite, and tin-based materials have been widely investigated. Sn can intercalate lithium up to Li/Sn atomic ratio of 4.4 with a theoretical specific capacity of 993 mAh g^{-1} [1], whereas graphite gives 372 mAh g^{-1}. Though tin is very attractive for its high specific capacity, low-cost and availability, the drastic volume change (about 300%) between Sn and $Li_{4.4}Sn$ causes electrode pulverization and loss of electric contact that is responsible for poor electrode cycle life [2]. Nanometric materials [3,4] and intermetallic compounds [5–7] have been the main strategies pursued to reduce this drawback and, recently, tin or tin oxide/carbon composites have aroused much attention because the carbon seems to enhance the tin's electrochemical stability [8–12]. However, the percentage of tin in the carbon composites is generally low, so that the benefit in terms of specific electrode capacity with Sn content lower than 50% (w/w) is scarce with respect to graphite electrodes. Furthermore, all the carbons display appreciable and stable lithium-insertion capacity at the potential range of the tin-based electrodes [13,14], thus making carbon an active lithium-intercalating component and, perhaps, the only one that remains stable over a high number of cycles. Carbon is responsible for large irreversible capacity at the first cycle, which is detrimental for electrode balancing in batteries.

It has also been reported that all-metal structured electrodes manufactured using three-dimensional current collectors [15] and nanowire technology [16–19] display enhanced performance with respect to conventional electrodes even in terms of cycling stability. Furthermore, the commercialization of Sony Nexelion™ lithium-ion battery [20] bearing a composite anode based on an SnCo amorphous alloy has attracted much attention in regard to the production of a tin-based anode with low crystallinity.

The present paper reports the synthesis and characterization of nanowires of SnCo alloy electrochemically grown inside the channels of polycarbonate membranes (SnCo-*PM*) and the results of repeated galvanostatic lithiation–delithation tests on these nanowire (NW) electrodes in conventional organic electrolyte for lithium ion batteries. The performance of the SnCo-*PM* is also compared to that of NWs of the alloy grown within anodic alumina membranes (SnCo-*AM*) [21,22].

2. Experimental

2.1. Preparations of SnCo NWs

Tin–cobalt alloy was electrodeposited inside the channels of a commercially available Whatman Cyclopore™ polycarbonate porous template that is a 20 μm thick track etched membrane with cylindrical pores of about 200 nm and a pore density in the order of 10^{12} m^{-2}. A gold film of few nanometers was sputtered on one side

* Corresponding author. Tel.: +39 051 2099798; fax: +39 051 2099365.
E-mail address: marina.mastragostino@unibo.it (M. Mastragostino).

0378-7753/$ – see front matter © 2010 Elsevier B.V. All rights reserved.
doi:10.1016/j.jpowsour.2010.09.039

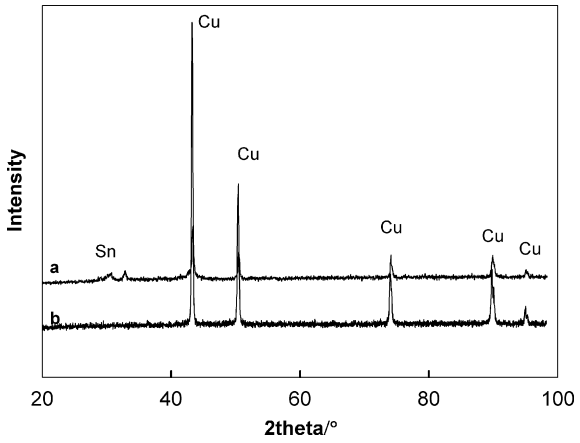

Fig. 1. Typical XRD pattern of SnCo alloy NWs after template removal (a). The XRD pattern of current collector alone is reported (b).

of the membrane before electrodeposition in order to make it conductive. The membrane was then glued with conductive paste to a holder specially designed for deposition of the Cu current collector and, hence, the tin–cobalt alloy NWs. The electrodepositions were carried out in a three electrode cell, with a Standard Calomel Electrode (SCE) as reference electrode and a platinum wire as counter electrode, using an EG&G Potentiostat/Galvanostat (mod. 273A).

The composition of the aqueous baths for deposition of the Cu current collector (bath 1) and the SnCo alloy (bath 2) was: $CuSO_4$ 2.0×10^{-1} M and H_3BO_3 1.0×10^{-1} M at pH 3.0 (bath 1) and $SnSO_4$ 2.0×10^{-2} M, $CoSO_4$ 5.0×10^{-3} M, Na_2SO_4 2.0×10^{-1} M and sodium gluconate (chelating agent) 2.0×10^{-1} M, at pH 4.6 (bath 2). A 15-μm thick Cu current collector was deposited under galvanostatic conditions at 20 mA cm^{-2} for 1 h at room temperature. The deposition of the SnCo alloy was carried out under potentiostatic conditions at −1 V (vs. SCE) and at 60 °C for 1 h; the SnCo NW arrays were washed in water and then in chloroform to completely dissolve the polycarbonate template membrane.

2.2. Structural, morphological and chemical characterization of SnCo NWs

Structural characterization of SnCo NWs was performed by X-ray diffraction (XRD) using a Philips generator (mod. PW 1130) working with the Cu Kα radiation (λ = 1.54 Å), and a PW 1050 goniometry. Morphology was investigated by a Field Emission Gun – Environmental Scanning Electron Microscope (FEG-ESEM, FEI Quanta™ 200F) equipped with an X-ray energy dispersive spectrometer (EDS). Elemental analysis was also performed by an inductively coupled Plasma/Optical emission spectrometer (ICP/OES, Perkin Elmer Optima™ 2100DV). Both techniques were used because EDS analysis yields local composition and ICP/OES the bulk composition of the sample to allow determination of active material mass.

2.3. Electrochemical characterization of SnCo NWs

Sn-Co NW electrodes (0.9-cm diameter disk) were tested in "T-type" electrochemical cells assembled in an argon-filled MBraun Labmaster 130 dry-box (H_2O and O_2 < 1 ppm). Lithium foils were used as both reference and counter electrodes and the latter was separated from the working electrode by a glass separator (Whatman GF/D 400 μm thick) soaked in the same electrolyte of the electrochemical cell, i.e. ethylene carbonate (EC): dimethylcarbonate (DMC) 1:1–1 M $LiPF_6$ (Ferro Corp). Electrochemical characterizations were performed by a Perkin-Elmer VMP multichannel potentiostat/galvanostat. The specific capacity values of the tested electrodes are referred to the tin's mass.

3. Results and discussion

The results of EDS and ICP analyses of the synthesized SnCo-*PM* alloy after template chemical dissolution indicate that the Sn molar fraction was 0.76 and the Sn loading per cm^2 of NW array was 1.1 mg. Fig. 1 shows an XRD pattern of the electrodeposited SnCo-*PM* after template dissolution. Given that all the intense diffraction peaks are due to the Cu current collector and only two very small, broad peaks at 30.64° and 32.92° are attributable to Sn or to an SnCo phase [5,23], the XRD analysis demonstrates that the electrodeposited SnCo alloy is amorphous.

Fig. 2 displays the SEM images of the SnCo-*PM* after template dissolution and shows that the NWs have a diameter of 0.2 μm and are 15 μm high. The population of these SnCo-*PM* is less dense than that of amorphous SnCo NWs (Sn molar fraction 0.64) grown inside alumina membranes, where the NWs had a diameter of 0.35 μm and were 3 μm high after template dissolution [21,22]. Differences in the template morphology must be carefully considered for application in Li-ion battery of SnCo NWs prepared by the template method; Fig. 3 shows the SEM image of the SnCo-*AM* after alumina dissolution for comparison.

Fig. 4 shows charge–discharge voltage profiles of the SnCo-*PM* electrode tested by deep galvanostatic cycles at 1 C-rate in the potential range 2.00–0.02 V, and Fig. 5 displays the electrode specific capacity values and cycle efficiency over 35 lithiation–delithiation cycles. The electrode specific capacity

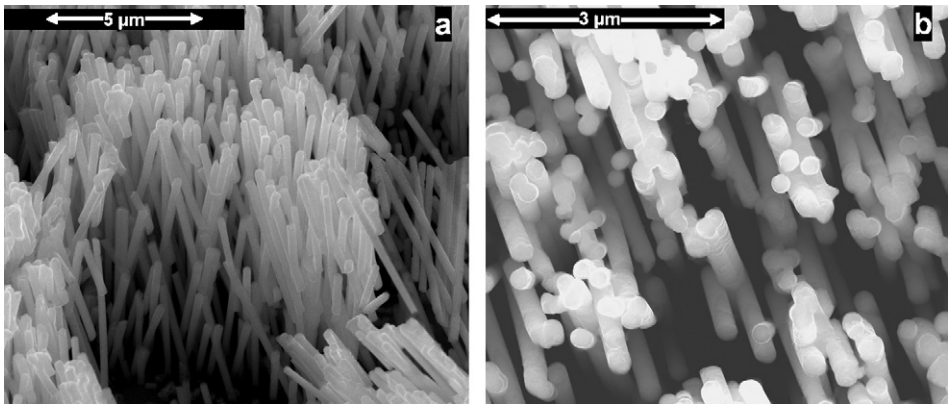

Fig. 2. SEM images of SnCo-*PM* after *PM* template dissolution at different magnifications. (a) Cross-section view, (b) top-down view.

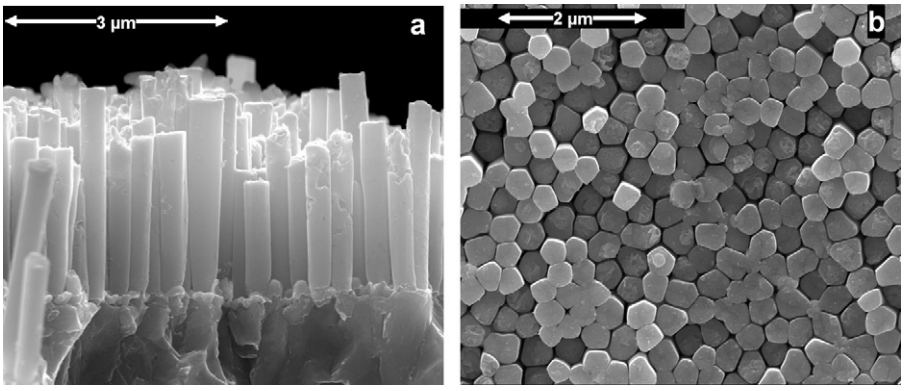

Fig. 3. SEM images of SnCo-*AM* after *AM* template dissolution at different magnifications. (a) Cross-section view, (b) top-down view.

referred to the tin mass was almost constant over cycling and approaches the Sn theoretical capacity, indicating that the $Li_{22}Sn_5$ alloy phase has been formed and that all the tin in the electrode is electrochemically active. Furthermore XRD measurement performed on cycled electrode (not reported here) demonstrated that the amorphous nature of the electrode material was maintained upon cycling. It is worth noting that the SnCo-*PM* electrode performs significantly better than recently reported tin-based electrodes [15,24–31] both in terms of specific capacity and cycling stability, and that the capacity of this electrode is about 1.0 mAh cm^{-2}, which is a very high value for nanowire technology [18].

These SnCo-*PM* electrodes display significantly better cycling stability than the SnCo-*AM* NW electrodes. Some voltage profiles over 20 galvanostatic lithiation–delithiation cycles at 0.1 C of the latter electrode are reported in Fig. 6. The figure shows that the SnCo-*AM* electrode delivers constant values of specific capacity (corresponding to *ca.* 900 mAh g^{-1} of Sn) over the first 12 cycles; an abrupt capacity fade occurs in a few cycles after this initial stability.

To investigate the effect of lithiation/delithiation cycles on the SnCo NW structures, the SEM images of the electrodes after cycling were acquired and are shown in Figs. 7 and 8 for the SnCo-*PM* and SnCo-*AM* electrodes, respectively. The nanowire structure of the SnCo-*PM* NW electrodes, unlike that of the SnCo-*AM* electrodes, is still recognizable after repeated cycles, thus indicating that the morphology of the SnCo-*PM* effectively offsets the enormous deformation that occurs in full lithiation of tin (4.4 Li/Sn), even though several wires became a compact mass of deformed

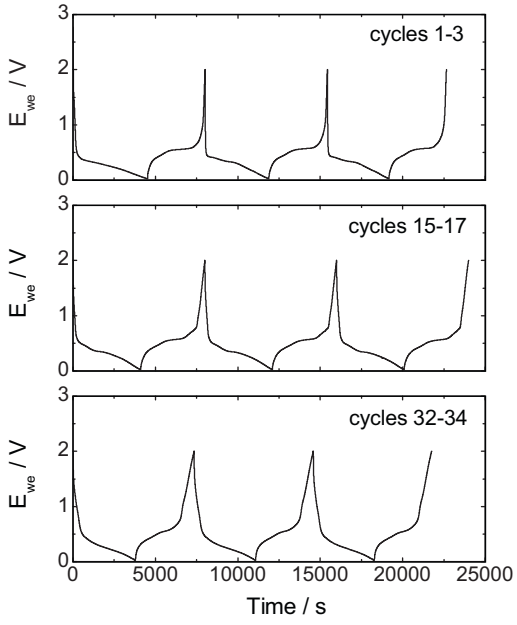

Fig. 4. Voltage profiles of some representative cycles of a SnCo-*PM* electrode cycled at 1 C and 30 °C.

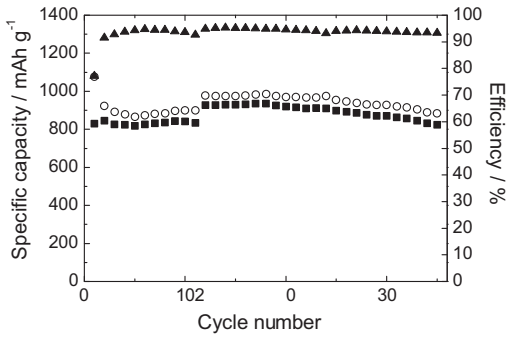

Fig. 5. Specific capacity and efficiency vs. cycle number of an SnCo-*PM* electrode cycled at 1 C and 30 °C. (◯) Lithiation, (■) delithiation and (▲) efficiency.

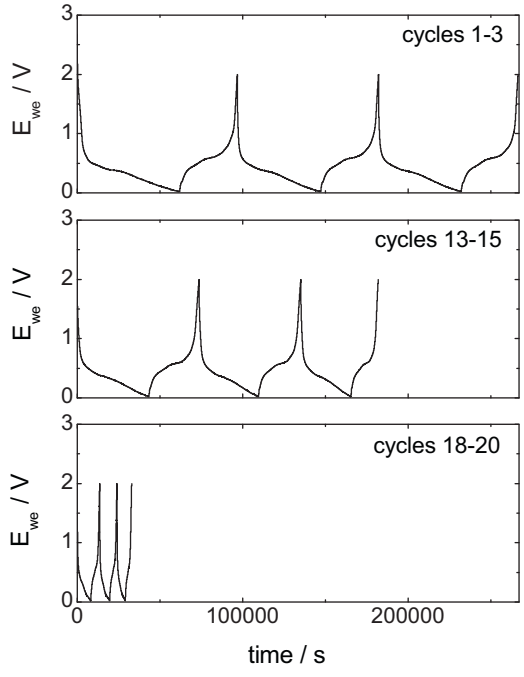

Fig. 6. Voltage profiles of some representative cycles of an SnCo-*AM* electrode cycled at 0.1 C and 30 °C.

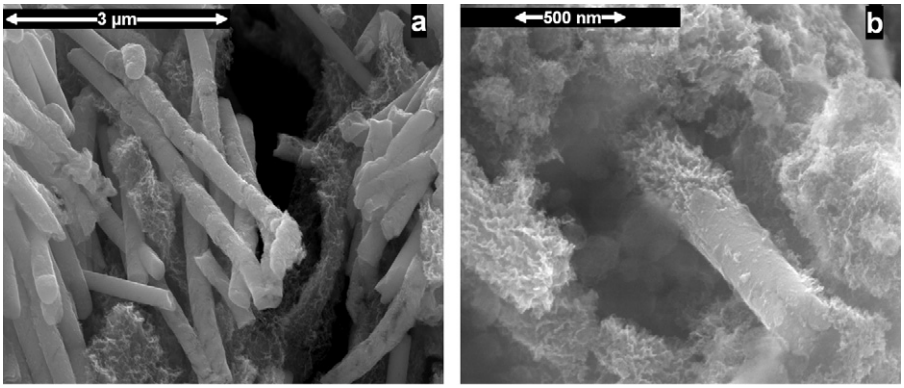

Fig. 7. SEM images of cycled SnCo-*PM* electrode at different magnifications.

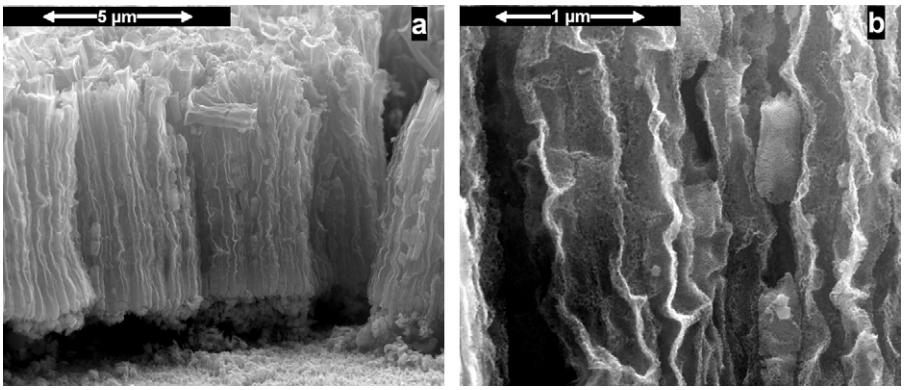

Fig. 8. SEM images of cycled SnCo-*AM* electrode at different magnifications.

porous structures. The SEM magnification in Fig. 7b gives a view of the deformation process of a single SnCo-*PM* nanowire.

Comparison with the SEM images of the SnCo-*AM* cycled electrodes demonstrates that NW size and distance are key parameters for durability of these electrode structures. The lack of free space causes the compaction of the nanowires and the increase of the expansion in the axial direction with consequent formation of horizontal cracks that are deleterious for maintaining contact with the current collector and, hence, for the electrochemical cycling stability of the electrode. The zoomed image in Fig. 8b shows that the SnCo-*AM* nanowires are deformed with lamellar extrusions caused by the extreme compression of the nanowires. The mechanical stress is not properly absorbed by these NW structures and the electrical contact with the current collector is compromised after a few cycles.

4. Conclusions

An array of amorphous SnCo nanowires fabricated by template electrodeposition in polycarbonate membrane template yielded electrodes capable of reversibly intercalating lithium up to $Li_{22}Sn_5$ for 35 cycles with an elevated capacity per cm^2 (ca. 1 mAh cm^{-2}). This promising result is related to a morphology of the electrode array that features free space among nanowires capable of buffering the mechanical stress of the lithiation–delithiation process. Comparison with the performance of electrodes based on SnCo nanowires grown inside alumina membranes demonstrates that the SnCo-*PM* morphology is more suitable than that of the SnCo-*AM* for stability over cycling. The optimization of NW technology in terms of nanowire size and distance should thus be a promising route to enhancing the mechanical strength and durability of tin-based electrodes.

References

[1] M. Winter, J.O. Besenhard, Electrochimica Acta 45 (1999) 31–50.
[2] L.Y. Beaulieu, K.W. Eberman, R.L. Turner, L.J. Krause, J.R. Dahn, Electrochemical and Solid State Letters 4 (2001) A137.
[3] A.H. Whitehead, J.M. Elliott, J.R. Owen, Journal of Power Sources 81/82 (1999) 33–38.
[4] C. Kim, M. Noh, M. Choi, J. Cho, B. Park, Chemistry of Materials 17 (2005) 3297.
[5] A.D.W. Todd, R.E. Mar, J.R. Dahn, Journal of The Electrochemical Society 153 (2006) A1998–A2005.
[6] A.D.W. Todd, P.P. Ferguson, J.G. Barker, M.D. Fleischauer, J.R. Dahn, Journal of The Electrochemical Society 156 (2009) A1034–1040.
[7] M.-G. Kim, J. Cho, Journal of The Electrochemical Society 156 (2009) A277–A282.
[8] K.E. Aifantis, S. Brutti, S.A. Hackney, T. Sarakonsri, B. Scrosati, Electrochimica Acta 55 (2010) 5071–5076.
[9] L. Zou, L. Gan, F. Kang, M. Wang, W. Shen, Z. Huang, Journal of Power Sources 195 (2010) 1216–1220.
[10] C.-L. Zhu, M.-L. Zhang, Y.-J. Qiao, P. Gao, Y.-J. Chen, Materials Research Bulletin 45 (2010) 437–441.
[11] F.M. Courtel, E.A. Baranova, Y. Abu-Lebdeh, I.J. Davidson, Journal of Power Sources 195 (2010) 2355–2361.
[12] J. Hassoun, G. Derrien, S. Panero, B. Scrosati, Advanced Materials 20 (2008) 3169–3175.
[13] E. Buiel, J.R. Dahn, Electrochimica Acta 45 (1999) 121–130.
[14] C. Arbizzani, S. Beninati, L. Damen, M. Mastragostino, IMLB 2010 Montreal (Canada), Abs. 25.
[15] Z. Du, S. Zhang, T. Jiang, Z. Bai, Electrochimica Acta 55 (2010) 3537–3541.
[16] C.K. Chan, H. Peng, G. Liu, K. McIlwrath, X.F. Zhang, R.A. Huggins, Y. Cui, Nature Nanotechnology 3 (2008) 31–35.
[17] J. Hassoun, S. Panero, P. Simon, L. Taberna, B. Scrosati, Advanced Materials 19 (2007) 1632–1635.
[18] L. Bazin, S. Mitra, P.L. Taberna, P. Poizot, M. Gressier, M.J. Menu, A. Barnabé, P. Simon, J.-M. Tarascon, Journal of Power Sources 188 (2009) 578–582.
[19] J.-H. Kim, S. Khanal, M. Islam, A. Khatri, D. Choi, Electrochemistry Communications 10 (2008) 1688–1690.
[20] Information on http://www.sony.net/SonyInfo/News/Press/200502/05-006E/.
[21] G. Ferrara, R. Inguanta, S. Piazza, C. Sunseri, Electrochemical and Solid-State Letters 12 (2009) K17–K20.
[22] G. Ferrara, R. Inguanta, S. Piazza, C. Sunseri, Journal of Nanoscience and Nanotechnology 10 (2010) 8328–8335.

[23] E. Gómez, E. Guaus, J. Torrent, X. Alcobe, E. Vallés, Journal of Applied Electrochemistry 31 (2001) 349–354.
[24] C. Li, W. Wei, S. Fang, H. Wang, Y. Zhang, Y. Gui, R. Chen, Journal of Power Sources 195 (2010) 2939–2944.
[25] R. Yang, J. Huang, W. Zhao, W. Lai, X. Zhang, J. Zheng, X. Li, Journal of Power Sources (2010), doi:10.1016/j.jpowsour.2010.04.069.
[26] R Yang, Y. Gu, Y. Li, J. Zheng, X. Li, Acta Materialia 58 (2010) 866–874.
[27] J. Li, D.-B. Le, P.P. Ferguson, J.R. Dahn, Electrochimica Acta 55 (2010) 2991–2995.
[28] B. Liu, Z.P. Guo, G. Du, Y. Nuli, M.F. Hassan, D. Jia, Journal of Power Sources 195 (2010) 5382–5386.
[29] X.-Y. Fan, F.-S. Ke, G.-Z. Wei, L. Huang, S.-G. Sun, Journal of Solid State Electrochemistry 13 (2009) 1849–1858.
[30] X.-Y. Fan, F.-S. Ke, G.-Z. Wei, L. Huang, S.-G. Sun, Journal of Alloys and Compounds 476 (2009) 70–73.
[31] J. He, H. Zhao, M. Wang, X. Jia, Materials Science and Engineering B 171 (2010) 35–39.